Interaction of a High-Power Laser Beam with Metal Sheets

C. D. Boley, K. P. Cutter, S. N. Fochs, P. H. Pax,
M. D. Rotter, A. M. Rubenchik, R. M. Yamamoto

July 13, 2009

Disclaimer

This document was prepared as an account of work sponsored by an agency of the United States government. Neither the United States government nor Lawrence Livermore National Security, LLC, nor any of their employees makes any warranty, expressed or implied, or assumes any legal liability or responsibility for the accuracy, completeness, or usefulness of any information, apparatus, product, or process disclosed, or represents that its use would not infringe privately owned rights. Reference herein to any specific commercial product, process, or service by trade name, trademark, manufacturer, or otherwise does not necessarily constitute or imply its endorsement, recommendation, or favoring by the United States government or Lawrence Livermore National Security, LLC. The views and opinions of authors expressed herein do not necessarily state or reflect those of the United States government or Lawrence Livermore National Security, LLC, and shall not be used for advertising or product endorsement purposes.

Interaction of a high-power laser beam with metal sheets[*]

C. D. Boley, K. P. Cutter, S. N. Fochs, P. H. Pax,

M. D. Rotter, A. M. Rubenchik, and R. M. Yamamoto

Lawrence Livermore National Laboratory

Livermore, CA 94551

Experiments with a high-power laser beam directed onto thin aluminum sheets, with a large spot size, demonstrate that airflow produces a strong enhancement of the interaction. The enhancement is explained in terms of aerodynamic effects. As laser heating softens the material, the airflow-induced pressure difference between front and rear faces causes the metal to bulge into the beam. The resulting shear stresses rupture the material and remove it at temperatures well below the melting point. The material heating is shown to conform to an elementary model. We present an analytic model of elastic bulging. Scaling with respect to spot size, wind speed, and material parameters is determined.

I. INTRODUCTION

The role of airflow in enhancing laser interactions with metals has been studied for some time[1-5]. In most cases, the enhancement is due to two factors. First, airflow removes the melted material, thus increasing the ablation rate. Second, airflow removes the oxide layer and provides an oxygen supply, thereby aiding the combustion process[3]. This paper analyzes an experiment in which a third mechanism -- aerodynamic pressure decrease -- plays a dominant role.

Our experiment involves the irradiation of thin sheets of aluminum by a 25-kW solid-state laser, with a large spot size, of order several cm. Airflow decreases the pressure on the front of the plate. While laser heating softens the material, the pressure difference causes the aluminum to bulge into the wind and thus into the incoming beam. The material is ruptured by the resulting shear stresses, leading to its removal by the airflow. This occurs at temperatures well below the melting point. Combustion is insignificant because a strong, dense oxide layer builds up on the aluminum surface.

Except for the presence of airflow, our experimental situation is similar to that involved in the irradiation of a pressurized aluminum container[6]. In our case, the data indicate that the important phenomena are elastic bulging, plastic flow, and breaking, rather than direct thermally induced cracking.

After reviewing the experiment, we discuss the overall behavior of target heating, bulging, and burn-through, on the basis of high-speed photography and thermocouple data. We show that the heating is adequately described by a simple model in which the volume beneath the beam fills up uniformly and steadily with heat. We then turn to an elastic analysis, modeling the softened material as an elastic plate subject to the pressure difference. We show that the model provides both a good description of the experiment and useful scaling for dependence on spot size, wind speed, and material parameters. Combining this model with burn-through information, we are able to make estimates for the elastic modulus and yield strength of the target at the burn-through temperature.

II. EXPERIMENT

The experimental setup[7] is illustrated in Fig. 1. Sheets of aluminum 6061 (thickness 0.18 cm) were irradiated by a solid-state heat-capacity laser operating at a

2

time-averaged power of about 25 kW and a wavelength of 1.064 μm. The laser produced pulses of approximately 125 J, at a pulse repetition rate of 200 Hz. The approximate pulse length was 0.5 ms. Since the pulse-to-pulse period was 5 ms, the duty factor was about 10%. The beam footprint was square, and the irradiance was practically uniform over the spot. Examination of the laser imprint after several pulses showed no visible patterns. According to calorimetry, the pulse-to-pulse energy varied by less than 5%.

The temperature response was close to that of a CW laser with the same average power. The reason is that the characteristic diffusion distance between pulses was of order $(4D\tau)^{1/2} \sim 0.1$ cm, where the thermal diffusivity has been estimated as $D \sim 1$ cm^2/s. This distance is small compared to the spot size of several cm. On the other hand, it is of the same order as the thickness of the sheet. Therefore temperature uniformity is established very rapidly through the target thickness, regardless of the pulse format. The temperature increase after one pulse was about a few degrees. This is negligible in comparison with the overall gradual temperature increase.

The wind blower generated airflow with a speed of about 100 m/sec along the surface. The samples were painted with a high-absorptivity paint. The diagnostics included thermocouples attached to the target rear side, infrared cameras, and high-speed cameras to observe the development of surface modifications.

III. OBSERVED BEHAVIOR

First we consider an experiment without airflow. Figure 2 shows a target having a spot size of 12x12 cm^2 (irradiance ~ 0.17 kW/cm^2), irradiated for 4 s. The sample exhibits both thermally induced cracking and melting, but there is no burn-through.

In contrast, airflow results in a dramatic burn-through during the same irradiation time, as shown in the right-hand part of Fig. 2. Here the spot size is 13x13 cm^2, which is somewhat larger than the case without airflow. The mechanism of breakup is clarified by the sequence of frames shown in Fig. 3. During the first second or so (before the first frame), the material is softened by the laser heating. Airflow decreases the pressure on the side of the incident beam by [✗], or about 0.06 bars. This sets up an elastic bulging, which is proportional to the ratio of the pressure to Young's modulus, as we show in the next section. The pressure is relatively small, but Young's modulus decreases markedly with temperature. For potential flow and small bulging, the pressure drop is uniform over the spot and the bulging is symmetric. If the bulging becomes sufficiently large, vortices begin to be formed, thus causing an asymmetry between the front and the rear of the bulge. The bulging is apparent even before 2 s, as seen in frame 1 of Fig. 3. Note that a small hole has formed on the downwind side of the target. We believe that this follows from the fact that the flow pattern over a bulge can lead to the formation of downwind vortices. These can increase the local pressure and cause large local shear stresses. For a smaller spot size, the bulging is less pronounced and the material breaks through in the center.

As the bulging increases, the stresses tear through the softened material, creating two holes (frames 2 and 3). These coalesce into a single large hole (frame 4) before the target is completely destroyed (frame 5). In the last three frames, one can discern the removal of macroscopic pieces of metal. Referring back to Fig. 1, we see that the screen has collected debris after the shot. The presence of large unmelted pieces of metal

confirms that the material destruction occurs below the melting point. Figure 4 shows sample debris collected at the screen.

Figure 5 shows the thermocouple traces for experiments with three spot sizes: 16x16 cm^2, 13x13 cm^2 (as above), and 9x9 cm^2. The thermocouple was placed at the center of the back side. In all cases, the traces reach a maximum (while the beam is still on) at temperatures well below the aluminum melting temperature ($T_m \sim 660$ C). Note, however, that the trace for the 13x13 cm^2 spot starts to decrease somewhat after 2 s. This cannot be a signal of burn-through, since we saw in Fig. 3 that a downwind hole had already formed somewhat earlier. We infer that the thermocouple remained attached to the coupon for a short time after the hole was formed. Thus the maxima of the thermocouple traces give an overestimate of the burn-through time.

Analytical estimates of the temperature development, ignoring burn-through phenomena, are also shown in Fig. 5. These are based on a simple model in which the temperature is assumed uniform through the slab, lateral heat transport is neglected (because the diffusion distance during a 4-s run is small compared to the spot size), and the beam is spatially flat. Radiative cooling is of the order of a few W/cm^2, which is negligible in comparison with the laser irradiance of greater than 100 W/cm^2. From turbulent boundary layer theory[8], the cooling rate due to airflow at the (ambient) temperature T_0 is $q = \beta\, k_B (T - T_0)$, where the heat transfer coefficient has the form

$\beta = [\gamma/(\gamma - 1)]\, n\, v\, F(\mathrm{Re})$, with n the air density, v the air speed, γ the adiabatic index, and $F(\mathrm{Re})$ a tabulated function of the Reynolds number of the airflow. Inserting appropriate

values, one finds that the cooling rate is of order several W/cm^2, which is small compared to the laser irradiance.

In a reasonable approximation, then, the beam steadily heats the volume beneath the irradiated spot, producing an aluminum temperature given by

$$T(t) = \alpha I t / h \rho C, \tag{1}$$

where α is the optical absorptivity, I is the laser irradiance, and ρC is the heat capacity per volume. As shown in Fig. 5, this simple model compares well with experiment while the thermocouple is attached. Here the material parameters are approximated by estimates halfway between room temperature and melting temperature ($\rho C = 2.8$ J/cm^3), and the absorptivity is taken as 0.8. The results indicate that the paint remains highly absorptive, without noticeable change of reflectivity, until the moment of break-through. This may be due to the relatively low break-through temperature. Two-dimensional thermal modeling with a temperature-dependent heat capacity and thermal conductivity, as in Ref. 7, produces results close to this simple model.

Because the sample is destroyed well below the melting temperature, airflow reduces the amount of energy needed to burn through the material. The fractional reduction in energy required for burn-through in comparison with the absence of airflow (when the sample must be melted) is $(T_m - T_b)/(T_m - T_0)$, where T_b is the burn-through temperature and T_0 is room temperature. Using a burn-through temperature of 400 C, we see that airflow reduces the required energy by about 40%.

IV. ELASTIC ANALYSIS

We now turn to a quantitative description of the observed bulging. Since the displacement of the surface is small even for large spots, we employ an elastic treatment. The elastic modulus of aluminum decreases rapidly with temperature. Consequently, even a small pressure difference will deform the material. Only the softened material is affected. Thus the situation can be viewed as the deformation of a thin, square membrane with clamped edges, subjected to uniform pressure, as illustrated in Fig. 6. Since the typical bulging time in our experiments (~ 1 s) is much longer than the sound transit time (~ 10^{-5} s), the deformation adiabatically follows the change in elastic modulus due to the temperature increase. It increases with time only through its parametric dependence on Young's modulus.

The deflection satisfies the biharmonic equation with a driving term proportional to the pressure and inversely proportional to Young's modulus[9,10]:

$$\nabla^2 \nabla^2 w(x, y) = \frac{12(1 - v^2)p}{E\,h^3} \; , \tag{2}$$

where v is Poisson's ratio (approximately 0.3 in our case, insensitive to temperature variations), and h is the thickness of the sample. From the linear pressure dependence, the deflection increases as the square of the wind speed.

Although our experiment has a square laser spot, it is instructive first to consider a round spot. Not only is the solution much simpler, but this is also a more typical experimental situation. In this case, the solution with a clamped edge works out to be[9]

$$w(r) = (3/16)\gamma R^4 [1 - (r/R)^2]^2 \, , \tag{3}$$

where $\gamma = (1-v^2)p/h^3E$ [dimensions of (length)$^{-3}$] and R is the radius. Note that the central deflection increases very rapidly ($\sim R^4$) with spot size. It is also sensitive to the metal thickness, varying as $1/h^3$. Thus from experiments with different spot sizes and the same thickness, we can rescale the results to situations with the same spot size and different thicknesses.

After evaluating the deformation tensor given by the deflection, one finds that the nonvanishing elements of the strain tensor are the radial strain e_{rr} and the hoop strain $e_{\theta\theta}$. Therefore the nonvanishing stresses are also radial and hoop. These are

$$\sigma_{rr} = \frac{2\sigma_0 z}{h}[1-(3-2v)(r/R)^2], \qquad \sigma_{\theta\theta} = \frac{2\sigma_0 z}{h}[1-(1+2v)(r/R)^2], \qquad (4)$$

where $\sigma_0 = (3pR^2/8h^2)(1-v)/(1-2v)$. It should be noted that the stresses are independent of Young's modulus. This is consistent with dimensional analysis, as the deflection equation (2) forces the stresses to increase linearly with pressure. In the stress formulas, the outer face of the bulging surface is located at $z = h/2$ and the inner face is at $z = -h/2$. Thus on the outer face, we see that the stresses are tensile at the center at the center and compressive at the edge, as expected. The tensile stress (radial or hoop) at the origin is just σ_0.

For a square spot, the above scalings continue to apply, but the solution is much more complicated. The clamped solution[10] can be written in the form

$$w(x,y) = \gamma a^4 \sum_m [f_m(\xi)g_m(\eta) + f_m(\eta)g_m(\xi)], \qquad (5)$$

where the spot size is taken as $2a \times 2a$, and the index m runs over the positive odd integers. Since the sum converges fairly rapidly, we require only the first few

dimensionless functions f_m and g_m. These are given in the Appendix. They depend on the dimensionless coordinates $\xi = x/a$ and $\eta = y/a$, which range between -1/2 and +1/2. Note that the scaling with respect to pressure, spot size, and thickness are the same as for the round spot, $w \sim pa^4/h^3$.

The normalized deflection is illustrated in Fig. 7. At the center of the plate, the deflection is approximately $0.0152\,\gamma\,a^4$. In comparison, a round spot of the same area has a central deflection of $0.0190\,\gamma\,a^4$, or about 25% greater.

The nonzero stress components are σ_{xx}, σ_{yy}, and σ_{xy}. The first two components are of primary interest to us, since the shear stress vanishes at the center of the plate. The *xx* component, on the outward bulging face, is

$$\sigma_{xx}(x,y) = -\frac{a^2 p}{2h^2} \sum_m \left\{ f_m''(\xi)g_m(\eta) + f_m(\eta)g_m''(\xi) + v[f_m(\xi)g_m''(\eta) + f_m''(\eta)g_m(\xi)] \right\}, \quad (6)$$

and σ_{yy} follows from symmetry. As in the case of the round spot, the outer stress is tensile at the center and compressive at the edge (cf. Fig. 8). It passes through zero at a normalized distance between 0.33 and 0.37, depending on the direction of the lineout. Note that the stress rises in the corners. The scaling agrees with that for the round spot, $\sigma \sim p(a/h)^2$.

From Fig. 3, we see that the maximum bulging before burn-through is $w_0 \sim 1$ cm. Using the aerodynamic pressure drop of 0.06 bars noted earlier, we infer that the value of Young's modulus at burn-through is about 4 kbar. This represents a dramatic decrease of more than two orders of magnitude from the room-temperature value of about 700 kbars. Note that this deflection implies a strain of order 10%, suggesting that the configuration

is beyond the assumed regime of small deformations. Nevertheless, we believe that our linear analysis is still reasonably reliable.

We take the point of view that burn-through occurs when the temperature-softened yield strength decreases to the point at which it satisfies the von Mises yield criterion[11] at the center:

$$. \tag{7}$$

Thus the yield strength at the elevated temperature is given by .

Since the sum in Eq. (6) is about -0.280 at the origin, we find $Y(T_b) \sim 60$ bars. This should correspond to the ultimate yield strength at the burn-through temperature of approximately 400 C. According to approximate data[12], the ultimate yield strength decreases from about 3 kbar to 0.2 kbar, as the temperature increases from ambient to the vicinity of 400 C (Fig. 9). Our estimated value is about 30% of the high-temperature value. The level of agreement seems reasonable, given the unknown accuracy of the data and uncertainties in detecting the time of burn-through, and hence the burn-through temperature.

According to our estimate, the ratio of the yield strength at burn-through to the yield strength at room temperature is about 0.02. We saw earlier that the corresponding ratio for Young's modulus was about 0.006. In typical constitutive models[13], the two quantities have similar temperature dependences. Because of the great uncertainties involved, however, the level of agreement estimated here is reasonable. One possible explanation of the smaller ratio for Young's modulus is that the observed deflection was enhanced by plastic effects.

Finally, let us review the applicability of our model. We have assumed that the temperature is uniform across the metal sheet. For this to hold, the sheet thickness must be much smaller than the thermal diffusion length $\ell = (4D\tau)^{1/2}$, where D is the metallic thermal diffusivity and τ is the irradiation time. Estimating $D \sim 1$ cm^2/s as in Sec. II, we have $\ell \sim 4$ cm at 4 s, which greatly exceeds the 1.8-mm thickness of aluminum. This length is also reasonably small compared to the spot size, indicating that lateral thermal transport is not important. These points are confirmed, of course, by the agreement of the point thermal model of Eq. (1) with experiment. A nonuniform temperature distribution would result in nonuniform softening, which would require a more complicated thermo-mechanical description. In addition, the sheet must be sufficiently thin to be heated to the softening temperature during the pulse, or $h < \alpha I \tau / \rho C(T_s - T_0)$, where T_s is the softening temperature. Taking $T_s \sim 400$ C, we see that h must not exceed 0.5 cm for a heating time of 4 s.

V. CONCLUSIONS

We have analyzed an experiment involving the large-spot irradiation of thin sheets of aluminum by a 25-kW solid-state laser, in the presence of airflow at Mach ~0.3. As the material is softened by beam heating, the small pressure difference due to airflow causes the target to bulge elastically into the wind. As a result, shear stresses rupture the material and lead to its removal, at a temperature below its melting point. Our observations are based on high-speed photography, thermocouple data, and target debris.
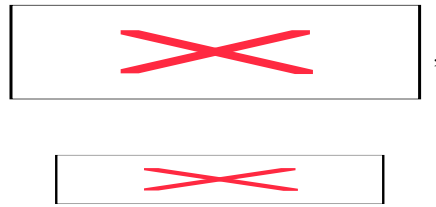
For a 13x13 cm^2 spot, photography indicates that the target is first penetrated somewhat downwind of the center. In our interpretation, this is caused by vortices associated with the bulging. The scaling of the elastic response with respect to spot size,

wind speed, and material parameters has been determined. The bulging is especially sensitive to spot size, increasing as a^4. One would expect a smaller target, exposed to the same irradiance, to rupture not through vortices but through material softening at the center. From thermocouple data, supplemented by an elementary thermal model, the burn-through temperature for the 13x13 cm^2 spot has been estimated to be approximately 400 C. From the calculated plate deflection, we have inferred an estimate of Young's modulus at the burn-through temperature. Similarly, the calculated stress has led to an estimate of the material strength at burn-through.

In summary, we have shown that airflow produces a strong enhancement, due to aerodynamic effects, of the interaction of a high-power laser beam with aluminum sheets. We have explained the experimental results by a quantitative analysis of the heating and elastic response of the metal. Experiments with other target materials, spot sizes, and wind speeds would be of great interest.

Appendix

The functions occurring in the formula for the deflection of a square, clamped plate under uniform pressure [Eq. (5)] are

,

$$g_m^{(a)}(\xi) = [\cosh \alpha_m - (1 + \alpha_m \tanh \alpha_m / 2) \cosh(2\alpha_m \xi) + \alpha_m \xi \sinh(2\alpha_m \xi)] / m^3 ,$$

$$g_m^{(b)}(\xi) = E_m \alpha_m [2\xi \sinh(2\alpha_m \xi) - \tanh \alpha_m \cosh(2\alpha_m \xi)],$$

where $\alpha_m = m\pi/2$. The first four constants in the last function are[10] $E_1 = 0.3722$,

$E_3 = -0.0380$, $E_5 = -0.0178$, and $E_7 = -0.0085$. We truncate the sum at four terms. If

the contribution $g_m^{(b)}(\xi)$ is dropped, the solution reduces to that of a simply supported

plate under uniform pressure.

References

[1]K. C. A. Crane, R. K. Garnsworthy, and L. E. S. Mathias, "Ablation of Materials Subjected to Laser Radiation and High-Speed Gas Flows," J. Appl. Phys. **51**, 5954-5961 (1980).

[2]Physical Sciences, Inc. (W. T. Laughlin, H. H. Legner, M. G. Miller, E. R. Pugh, and G. A. Simons), "Laser Materials Effects and Lethality Handbook," PSI-1302/TR-1615 (1999).

[3]A. M. Prokhorov, V. I. Konov, I. Ursu, and I. N. Mihailescu, "Laser Heating of Metals," Adam Hilger, 1990.

[4]W. M. Steen and K. Watkins, "Laser Materials Processing," Springer, London, 2003.

[5]N. V. Karlov, N. A. Kirichenko, and B. S. Luk'yanchuk, "Laser Thermochemistry: Fundamentals and Applications," Cambridge International Science, Cambridge, 1999.

[6]H. Mirels, and K. L. Zondervan, "Pulsed-Laser-Induced Vibration of Pressurized Thin Walled Cylinder**,"** AIAA Journal **44**, 128-135 (2006).

[7]C. D. Boley, S. N. Fochs, and A. M. Rubenchik, "Large-Spot Material Interactions with a High-Power Solid-State Laser Beam," J. Directed Energy **3**, 15-24 (2008).

[8]L. D. Landau and E. M. Lifshitz, "Fluid Mechanics," Pergamon Press, 1978.

[9]L. D. Landau and E. M. Lifshitz, "Theory of Elasticity," 3rd Edition, Pergamon Press, Oxford, 1986.

[10]S. Timoshenko and S. Woinowsky-Krieger, "Theory of Plates and Shells," 2nd Edition, cGraw-Hill Book Company, Inc., New York, 1959. References to the original literature are given here.

[11]H. Ford and J. M. Alexander, "Advanced Mechanics of Materials," Longmans, Green and Co., London, 1963.

[12]Aluminum Association, Inc., "Aluminum Design Manual," 3rd Ed., Jan. 2005.

[13]D. J. Steinberg, S. G. Cochran, and M. W. Guinan, "A Constitutive Model for Metals Applicable at High Strain Rate," J. Appl. Phys. **51**, 1498 (1980).
Figure Captions

Figure 1. Experimental setup, immediately after irradiation of a sample. The laser is out of view, to the lower right. The designated elements are: (a) beam path, (b) blower assembly, (c) target (in this case, a 13x13 cm^2 spot size), (d) coupon pieces on a screen, (e) suction assembly.

Figure 2. Two samples irradiated for 4 s. Left: 12x12 cm^2 spot, without airflow. Right: 13x13 cm^2 spot, with airflow.

Figure 3. Successive stages in the burn-through of a 13x13 cm^2 aluminum sample. The wind is from the left. The time of the first frame is 1.67 s after the beam was turned on. The time between frames is about 160 ms.

Figure 4. Sample coupon debris collected at the screen. Note the solid (unmelted) pieces of metal.

Figure 5. Thermocouple traces and thermal model results for three spot sizes: 16x16 cm^2 (red), 13x13 cm^2 (green), and 9x9 cm^2 (blue). The thermocouple traces are jagged, while the model results are straight lines. The experiments have various conventions for $t = 0$.

Figur 6. Geometry of the elastic model (not to scale).

Figure 7. Calculated deflection of the target, versus normalized position for a square spot. The right-hand figure gives the horizontal (or vertical) lineout. The full line corresponds to a clamped plate, while the dashed line shows a freely supported plate. The deflection is normalized by [✗].

Figure 8. Calculated stress σ_{xx} on the outer face of the target, versus normalized position for the rectangular spot. Full line on the right: horizontal lineout; dashed line: vertical lineout. The stress is normalized by $p\,a^2/h^2$.

Figure 9. Ultimate tensile strength (red line) and yield tensile strength (full black line) of Al6061, as functions of temperature, from Ref. 12. The data are acknowledged to be subject to large uncertainties. The yield stress estimated from target experiments is about 0.06 kbars (arrow).